A new RNase sheds light on the RNase/angiogenin subfamily from zebrafish

Pizzo Elio, Antonello Merlino, Mimmo Turano, Irene Russo Krauss, Francesca Coscia, Anna Zanfardino, Mario Varcamonti, Adriana Furia, Concetta Giancola, Lelio Mazzarella, et al.

TITLE: A new RNase sheds light on the RNase/angiogenin subfamily from zebrafish

Authors: Elio PIZZO[*], Antonello Merlino[†,‡], Mimmo Turano[*], Irene Russo Krauss[†], Francesca Coscia[†], Anna Zanfardino[*], Mario Varcamonti[*], Adriana Furia[*], Concetta Giancola[†], Lelio Mazzarella[†, ‡], Filomena Sica[†, ‡], Giuseppe D'Alessio[*]

[*]Dipartimento di Biologia Strutturale e Funzionale, [†] Dipartimento di Chimica, Università di Napoli Federico II, Complesso Universitario Monte S. Angelo, Via Cinthia, I-80126 Naples, Italy, [‡]Istituto di Biostrutture e Bioimmagini, CNR, Via Mezzocannone 16, I-80134 Naples, Italy

Correspondence: dalessio@unina.it

The abbreviations used are: ZF-RNase, RNase from zebrafish; hANG, human angiogenin; RNase A, bovine pancreatic ribonuclease A; CD, circular dichroism; DSC, differential scanning calorimetry; Δf_D the fraction of denatured protein calculated from the ellipticity values obtained by circular dichroism analyses; RT-PCR, reverse transcription polymerase chain reaction; BSA, bovine serum albumin.

Short title: Zebrafish RNases

ABSTRACT

Only recently extracellular RNases of the RNase A superfamily, with the characteristic CKxxNTF sequence signature, have been identified in fish. This has led to the recognition that these RNases are present in the whole vertebrate sub-phylum. In fact, they comprise the only enzyme family unique to vertebrates. Four RNases from zebrafish (*Danio rerio*) have been previously reported, with a very low RNase activity, some endowed, like human angiogenin, with powerful angiogenic and bactericidal activities. Here we report the three-dimensional structure, the thermodynamic behaviour, and the biological properties of a novel zebrafish RNase, ZF-RNase-5. The investigation of its structural and functional properties, extended to all other sub-family members, provides an inclusive description of the whole zebrafish RNase sub-family.

INTRODUCTION

Only recently, when a large number of sequences of fish DNA and proteins has become available, it has been possible to recognize in fish proteins the unmistakable signature of an RNase sequence (CKxxNTF). It has thus become clear that RNases from the "RNase A Superfamily" are present not only in tetrapods, but also in fish, hence in all vertebrates. This has led to the proposal to rename the superfamily as the "Vertebrate RNase Superfamily" [1], a proposal in line with the relevant finding that a single family of enzymes has been recognized as present exclusively in the subphylum of vertebrates: that of RNases [2].

Several fish RNases have been identified and studied: four recombinant RNases from zebrafish (*Danio rerio*) [3-5] and two from salmon (*Salmo salar*) [6]. All fish RNases studied so far have a weak RNA degrading activity, and most of them are effectively angiogenic. As in the case of human angiogenin (hANG), their angiogenic activity is strictly dependent on the integrity of the enzyme catalytic activity [5,6]. On the other hand, all fish RNases studied so far have been found to be endowed with a bactericidal activity [3,6]. Surprisingly however, the latter activity, when investigated with salmon RNases, has been found to be maintained when the RNases are either catalytically inactivated or fully denatured [6].

In the last decade, hANG has been assigned various key biological roles, besides that of an angiogenic effector, such as regulation of proliferation of endothelial and cancer cells, stimulation

of rRNA transcription, stimulation of neurite outgrowth and pathfinding of motor neurons [7], control of stress-induced translational arrest [8,9].

RNases from zebrafish (ZF-RNases) have been independently studied in different laboratories. Three zebrafish RNases (ZF-RNase-1, -2 and -3) have been reported by Pizzo *et al.* [5]; two of them, plus a third, different enzyme, have been studied by Cho and Zhang [3]. Kazaukou *et al*. [4], after an extensive survey of zebrafish DNA sequences, which indicated widespread polymorphism among the known ZF-RNase homologues, produced the X-ray structure of two of the RNases (RNase-ZF-1a, and -3e). An assessment of the nomenclatures of the available zebrafish RNases is presented in Table 1. The Table includes a novel ZF-RNase-5 member, encoded by a gene sequence described by Kazakou *et al*. [4] as due to polymorphism (see below). The nomenclature of ZF-RNases as first proposed by Pizzo *et al*. [5], and its extension, will be used throughout this paper.

The expression during development and in adult animals of some ZF-RNases has been investigated by different laboratories with diverse results [3,10]. This approach is of special interest, given the possibility that zebrafish offers as a model experimental system for the studies of angiogenesis development, an approach already successfully explored [11-13].

A recent study [14] has revealed that ZF-RNase-1 and -2 are able to induce phosphorylation of extracellular signal-regulated kinase 1/2-mitogen-activated protein kinase. Furthermore, they undergo nuclear translocation, as hANG does, and accumulate in the nucleolus where they stimulate rRNA transcription.

Given the interest for the diverse bioactivities of zebrafish RNases, and the expediency of zebrafish as a model experimental system, especially for angiogenesis studies, we deemed of interest to prepare and characterize a novel ZF-RNase, ZF-RNase-5. Based on its amino acid sequence, this RNase has been previously proposed [4] as a polymorphic variant of the gene encoding ZF-RNase-2. We investigated the 3D structure of the protein, its thermodynamic behavior, and its biological profile, and concluded that ZF-RNase-5 is a protein and effector distinct from ZF-RNase-2 and all other ZF-RNases. As the investigation of ZF-RNase-5 properties has been extended to those of the other ZF-RNases, an inclusive description has emerged of the whole zebrafish RNase sub-family.

RESULTS

The primary structure of ZF-RNase-5

The expression of ZF-RNase-5, and its purification as a recombinant protein, are described in Experimental Procedures. The protein amino acid sequence is illustrated in Figure 1, in comparison with the sequence of all other ZF-RNases, hANG and RNase A. ZF-RNase-5 contains in its primary structure the classical RNase signature (CKxxNTF), and the His and Lys residues essential for catalysis are located at positions corresponding to those present in the other active RNases from the vertebrate superfamily. There are 34 amino acid substitutions in the sequence of ZF-RNase-5 with respect to that of ZF-RNase-2, 10 of which conservative. This gives a 73% identity, higher than the identity values between ZF-RNase-5 and the other ZF-RNases, which are in the 30-60% range.

The 3D structure of ZF-RNase-5

The 3D structure of ZF-RNase-1 (ZF1_pH8) and that of ZF-RNase-3, obtained at basic pH, have been described by Kazakou *et al*., [4]. We focused our attention on the structure of the newly identified ZF-RNase-5. Furthermore, we inspected new crystal forms of ZF-RNase-1, and analysed by homology modelling ZF-RNase-2 and -4. The structural models are shown in Figure 2, whereas the superimposition of their C alpha atoms is reported in Figure S1.

The crystal model of ZF-RNase-5 (residues 1-121) was refined to an R-factor of 17.8 % (R-free 21.0 %) at 1.8 Å resolution. A summary of the refinement statistics is presented in Table 2. In comparison to the previously described ZF-RNases (-1 and -3) [4] and hANG (PDB CODE 1ANG), the rmsd of the corresponding Cα atoms are 0.70 Å, 0.91 Å and 1.28 Å, respectively.

We found that among the zebrafish proteins, the most relevant differences are located in helix II. In ZF-RNase-5 this helix, which encompasses residues 24-35, has a first turn in a 3_{10} conformation, and terminates with a turn in a π helix conformation with main chain hydrogen bonds Met31-Ile36 and Ser32-Lys35 and Lys35 in the Lα conformation. In the corresponding region (residues 23-36) of ZF-RNase-1 [4] the network of hydrogen bonds (Ile30-Ile37 and Gly31-Lys36) is spatially conserved. Lys36 is in the Lα conformation, while the intervening extra residues Pro32 and Asn33 bulges out of the helix, forming a type I beta-bend (supplemental Figure S2). Thus the topology of this fragment is substantially unchanged with respect to ZF-RNase-5, although the insertion of the two residues formally breaks the helix at the level of Ile30 (Figure 2 and supplemental Figure S3). In the case of ZF-RNase-3 (residues 23-35) [4] the first turn of the helix is highly distorted.

ZF-RNase-5 is the first structure of a zebrafish RNase that presents a sulphate ion in P1; its interactions with the surrounding catalytic residues (His17, His117 and Lys45) and structured water molecules are similar to those found in RNase A (see e.g. [15] and other angiogenins [16,17]) (Figure 3A). The similarity of the active site architecture with that of RNase A extends to the subsite P2 where Lys12 and Arg15 are the analogues of Lys7 and Arg10 in the bovine pancreatic enzyme. However, in ZF-RNase-5 the B1 subsite delimited by Val47, Thr49, and Tyr118, is obstructed by that part of the C-terminal residues which is visible in the electron density map (119-122). In particular, the side chain of Glu120 makes two hydrogen bonds with Thr49 and partly mimics the binding interactions of the pyrimidine base. In the present case, the orientation of the Glu side chain is enforced by the involvement of this residue in a pseudo type II' beta-bend stabilized by a C_{10} hydrogen bond between the side chain of the preceding Asp119 and Gly121 (Figure 3B).

In order to investigate whether the different behaviour in the sulphate binding between ZF-RNase-5 and ZF-RNase-1 and -3 was not merely a result of differences in the environmental parameters used in the crystallization trials, we extended our analysis to crystals of ZF-RNase-1 grown at acidic pH and in the presence of an elevated concentration of SO_4^{2-} ions. This produced a new crystal form that contains two molecules in the independent unit (chains A and B). The crystals obtained at pH=4.5 were also equilibrated at pH=7.3 and the structure at the two pH's were refined independently (ZF1_pH4.5 and ZF1_pH7.3). It must be recalled here that the recombinant protein lacks the first three residues in the sequence [4]. To simplify the comparison with ZF1_pH8 the numbering of the latter has been maintained. The electron density map is very well defined for most of the protein residues. A summary of the refinement statistics is presented in Table 2. The C_α atomic positions for the two molecules in the asymmetric unit do not differ significantly and their rmsd is 0.42 Å at pH 4.5 and 0.41Å at pH 7.3.

The main structural differences between ZF1_pH4.5 and ZF1_pH7.3 are limited to solvent molecules and to the conformation of few side-chains. The inspection of the electron density maps of ZF1_pH4.5 reveals that chain A binds five sulphate ions and chain B binds three sulfates and one acetate ion. Details of the interactions of these ions with the protein are reported in Table S1. The binding site of a sulphate (acetate in molecule B) and that of a second sulphate are well conserved in both chains. The remaining non-equivalent sites are involved in packing contacts. The map of the anionic binding sites is strictly conserved in the structure at neutral pH, with the only exception of the acetate that is replaced by an additional sulphate anion. Thus, in contrast to numerous crystallographic reports on RNase A [15,18] and other members of the family [19-21], and angiogenins [16,17], and despite the relatively high concentration in the crystallization mixture, none of the sulphate ions is located in the active site, as the anion binds preferentially to other regions of ZF-RNase-1. The putative binding subsite B1 of the pyrimidine base is partially obstructed by the side chain of Glu122 located in the C-terminal segment of the protein. The

position of this residue, fixed by a hydrogen bond to Thr52, is common to all the angiogenins that have a Glu residue in the equivalent position and, in particular, to ZF1_pH8 [4]. Interestingly, the C-terminal segment, to which Glu belongs, is also the region where the largest differences are observed between the structure at basic pH and those at lower pH. In the latter, this region is better defined, probably due to packing interactions involving residues 125-127. On the overall, the C-terminus causes an obstruction of B1 that is even greater than that produced in ZF1_pH8

Physicochemical properties of ZF-RNase-5 and the other ZF-RNases

The conformational stability of recombinant ZF-RNase-5 was investigated by circular dichroism (CD) and differential scanning calorimetry (DSC), and compared with those of the other ZF-RNases, human angiogenin (hANG), and non-angiogenic RNase A, the RNase superfamily prototype.

When the thermal unfolding of the RNases was monitored by CD spectroscopy at 222 nm (Figure 4), melting curves with sigmoid profiles were obtained. The melting temperatures, T_m, of ZF-RNase -5 was found to be close to those of ZF-RNase-2, -4 , hANG and RNase A, whereas ZF-RNase-1 and -3 exhibited melting temperatures about 8-9 degrees lower (see Table 3). The denaturation enthalpy changes, $\Delta H^0_{vH.}$, calculated from the CD melting curves with the van't Hoff equation (see Experimental Procedures) are shown in Table 3. The equation describes two-state N↔D transitions, where N and D represent the native and the denatured state, respectively.

By DSC measurements, good agreement was established between the calculated melting temperatures and those found in CD experiments, as well as between the denaturation enthalpies ΔH^0_{cal}, directly measured from the DSC curves, and those measured with the van't Hoff equation (see Table 3). These data confirmed that the thermal denaturation process is for all the proteins a two-state transition process. The enthalpy value for ZF-RNase-5 was found to be close to those of ZF-RNase-1 and -3 and lower than the value obtained for hANG (about 50 kJ mol^{-1}). The enthalpy values for ZF-RNase-2 and 4 were instead close to the ΔH^0_{cal} of hANG and lower than the value found for RNase A.

In addition, as the denaturation of the RNases, followed by CD or by DSC, was found to be a reversible process at thermodynamic equilibrium, the entropy and Gibbs energy could be calculated. In Supplemental Figure S4 CD spectra and CD melting profiles illustrate the reversibility of the unfolding processes. Reversibility of unfolding for RNase A [22] and human angiogenin [23] has been previously described.

The entropy change values showed the same trend of the enthalpy change values (Table 3): the ΔS^0_{cal} value ΔS^0_{cal} of ZF-RNase-5 was determined to be close to that of ZF-RNase-1 and -3 and lower than the value obtained for hANG, whereas ΔS^0_{cal} values ΔS^0_{cal} of ZF-RNase-2 and -4 were determined to be close to that of hANG. An inspection of Gibbs energy values ΔG^0_{298} (listed in Table 3), showed that the thermodynamic stability of ZF-RNase-5 and all ZF-RNases falls in the range of 21-29 kJmol^{-1}, a stability close to that of hANG and far from that of RNase A.

The conformational stability of ZF-RNases against the denaturing action of urea was also investigated using two different spectroscopic methodologies: circular dichroism, that reflects conformational changes of the secondary structure, and steady-state florescence, to analyze conformational changes of the tertiary structure.

Very similar values of $C_{½}$, the urea concentration at half-completion of transition, were obtained by CD and fluorescence measurements for each protein, as shown in Table 3. The results of these experiments indicated that upon denaturation a simultaneous collapse occurs: of both secondary and tertiary structures. Furthermore, it confirms that the urea-induced unfolding of all the proteins is a two-state denaturation process, involving only native and denatured states. The value of $C_{½}$ of ZF-RNase-5 was comparable with that of ZF-RNase-4 and hANG, whereas

the $C_{½}$ of ZF-RNase-2 was found to be the highest among ZF-RNases. The values of $C_{½}$ of ZF-RNase-1 and -3 were found to be the lowest among the investigated ZF-RNases.

In conclusion, the stability against urea follows the same trend of thermal stability and confirms that ZF-RNase 1 and -3 have less stable native structures. They also indicate that ZF-RNase-5 and -2 have significantly different structural stabilities, thus suggesting that they are distinct proteins.

The ribonucleolytic, angiogenic and bactericidal activities of ZF-RNase-5

Zebrafish RNase-5, like the other fish RNases studied so far [3-6], is characterized by a low ribonucleolytic activity. This is not surprising, given its ability to act as an angiogenin (see below), and the typical low RNase activity of angiogenins. For measuring the activity, a continuous, very sensitive assay was chosen [24], previously proposed [25] as particularly suitable for measuring the low activity values of angiogenins and for a comparison of the activities of several RNases/angiogenins.

When the activity of ZF-RNase-5 was compared to those of the other ZF-RNases, hANG and RNase A, by performing assays in parallel, ZF-RNase-5 was found to be much less active than RNase A, the superfamily prototype, and roughly as moderately active as hANG and the other ZF-RNases (see Table 4). It should be noted that ZF-RNase-5 was found to be by 2 orders of magnitude more active than ZF-RNase-2: $k_{cat}/K_m = 1.25 \pm 0.09 \cdot 10^4$ versus $k_{cat}/K_m = 1.91 \pm 0.13 \cdot 10^2$).

With a standard, 2-dimensional assay, ZF-RNase-5 was found to be as angiogenic as hANG, as shown in Figure 5. In the Figure the results are also shown of angiogenic assays on ZF-RNase-4, never assayed before. As we have reported [5,6] for the previously investigated ZF-RNases, we found that also ZF-RNase-5 and -4 lost their angiogenic activity when their RNase activity was obliterated (data not shown).

ZF-RNase-5 was found to possess a strong bactericidal activity on Gram-negative bacteria (*Escherichia coli* and *Pseudomonas aeruginosa* were tested), and no activity on Gram-positive *Staphylococcus aureus* and *Bacillus subtilis* (see Figure 6*)*. Identical results were obtained with ZF-RNase-4, with LD50 value (the concentration required for a 50% effect) in the 0.75-1.0 μM range for both RNases. ZF-RNases -1, and -3 instead were found to possess a low to weak, but significant activity also on Gram-positive bacteria, while ZF-RNases-2 was found to be very active on these bacteria. The latter finding is of interest, because ZF-RNase-5, proposed to be a variant of ZF-RNases-2, has no activity on Gram-positive bacteria.

It may not be surprising that the bactericidal activity of ZF-RNase-5, like that of the other ZF-RNases, is conserved when the ribonucleolytic activity of the RNases is suppressed by alkylation of the catalytically essential His residues (see Experimental Procedures). Surprising is instead the finding that their bactericidal activity is conserved also when the structure of the RNases is unfolded, either by heating or by reduction of the protein disulfides and alkylation of the freed sulfhydryls [6,26] (data not shown).

ZF-RNase-5 in development

Given that zebrafish is a most convenient experimental model, especially for embryogenesis studies, and particularly for angiogenesis, and the availability of the zebrafish angiogenin genes and proteins described in this paper, we investigated the temporal expression profile of ZF-RNase-5 during embryonic/larval development. We found that the RNase was found to be expressed at all stages of development. As conflicting results have been reported for the other previously investigated ZF-RNases [3,10], we decided to assay or re-assay in parallel all the known ZF-RNases.

As illustrated in Figure 7, we confirmed the lack of expression in development of ZF-RNases -2 and -4, but found a strong expression of ZF-RNase-1 and -3, especially for the ZF-RNase-3 gene at 48 h after fertilization. In particular, the data in Figure 7 show that ZF-RNase-2 has no role in embryogenesis, whereas ZF-RNase-5, purportedly a variant of ZF-RNase-2, is present during the whole period of development.

DISCUSSION

To date four members have been studied in the zebrafish subfamily of the vertebrate RNase superfamily, and in part characterized: ZF-RNase-1, -2, -3, -4, all isolated as recombinant proteins [3-5,10,14]. A fifth member, ZF-RNase-5, is proposed here to be a cell product by itself, rather than a polymorphic variant of ZF-RNase-2 as previously suggested [4]. This proposal is supported by several lines of evidence:

1. The enzymatic activity of ZF-RNase-5 is 2 orders of magnitude higher than that of ZF-RNase-2.
2. The bactericidal activity on Gram-positive bacteria is absent in ZF-RNase-5, but quite strong in ZF-RNase-2.
3. ZF-RNase-2 is not expressed in development, whereas ZF-RNases-5 is strongly expressed in the whole development period.
4. The denaturation enthalpic and entropic values determined for ZF-RNase-2 are close to those of hANG, whereas those determined for ZF-RNase-5 are much lower. Urea denaturation experiments also indicate that ZF-RNase-2 is much more stable than ZF-RNase-5.

ZF-RNase-5 has been crystallized and its structure, determined by X-ray crystallography, has been directly compared with that of ZF-RNase-2 and -4, deduced through modeling, and the crystallographic models of ZF-RNase-1 and -3. With the due caution required when comparing structural and functional differences between proteins having significant differences in the amino acid sequence, some general trends can be extracted from the structural features of the different members of the subfamily.

Based on their structural homology with RNase A, putative substrate binding subsites, previously identified in angiogenins, can be identified also for ZF-RNases. The B1 and B2 subsites interact specifically with bases, whereas P0, P1, and P2 subsites interact with phosphate groups. Although the geometry of the P1 subsite is strictly conserved among ZF-RNases, it should be noted that only ZF-RNase-5 binds a sulphate in this subsite. This result is enforced by the fact that Zf-RNase-5 crystals were grown from solutions with a low ammonium sulphate concentration (0.2 M). This feature is probably related to a cluster of positive charges (Arg9, Lys12 and Arg15) in the proximity of the ZF-RNase-5 active site. In particular, Lys12 and Arg15 correspond to Lys7 and Arg10 of RNase A, two residues that line the P2 subsite and are considered to be important for substrate binding [27].

An important role in determining the low catalytic activity of angiogenins in comparison to RNase A has been ascribed to the obstruction of the B1 subsite that occurs in most angiogenins [16,28,29]. In these molecules a Glu/Gln residue on the C-terminal tail protrudes in the B1 subsite and forms two hydrogen bonds with the Thr involved in the pyrimidine base recognition. This feature is also observed in ZF-RNase-5. In this protein, as for hANG, the Glu residue is involved in a pseudo type II' beta-bend stabilized by a hydrogen bond between the amide nitrogen of Gly121 and the side chain of Asp119. This structural motif, which further restricts the conformational space available to the Glu residue, is not found in ZF-RNase-1, where the Asp residue is replaced by a His. In this respect, it should be recalled that the corresponding aspartate of RNase A (Asp121) forms a sort of "catalytic dyad" with His119 [30]. In the bovine pancreatic enzyme, the H-bond between the side chains of these two residues stabilizes the histidine conformation that is supposed to be active during the transphosphorylation step. In ZF-RNase-5, just like in hANG, no interactions between the corresponding Asp and His are observed, and Asp is engaged in the two enzymes in interactions with Ser118 and Gly121, respectively. However, it should be noted that a rotation of the Asp side chain from the *t* to g^- conformation would bring the carboxylate group in a position to form the hydrogen bond with the catalytic histidine. Moreover, the rotation of the aspartic side chain also results in the disruption of the hydrogen bond with the second residue next along the chain (Gly121 in ZF-RNase-5). This would also destabilize the position of the C-terminal residue and favour the expulsion of Glu120 from the B1 subsite (Figure 3B). This structural feature,

together with the greater ability of ZF-RNase-5 to bind in the active site a sulphate anion, may account for the enhanced enzymatic activity of the latter with respect to ZF-RNase-1.

It should be noted that the most relevant differences between ZF-RNases and hANG are localized at the C-terminal tail. In hANG, this region adopts a well defined 3_{10} helix conformation, which is anchored to the protein core by hydrophobic interactions involving residues downstream to the obstructive Gln117 (Ile119 and Phe120). In ZF-RNases the C-terminal segment seems to be much more mobile. Indeed, in ZF1_pH8 it is partially disordered and the part visible in the electron density map assumes a different conformation when compared to that observed in the structures of ZF1_pH4.5 and ZF1_pH7.3 here reported. In fact, in ZF-RNase-5 the C-terminus appears even more disordered: the last visible residue in the electron density map is Gly121. This could be reflected in an increased capability of ZF-RNase-5 to adopt an alternative conformation of the C-terminal tail that allows the binding of substrate.

Interestingly, despite ZF-RNase-2 shares a 73% of sequence identity with ZF-RNase-5, its catalytic activity is 100-fold lower. This result could be ascribed to a lower number of basic residues in the active site region of ZF-RNase-2 in comparison to ZF-RNase-5. Moreover, the putative B2 subsite of the former enzyme appears to be less accessible as a result of the presence of Arg107 replacing Gly109 in the latter. Concerning ZF-RNase-4, the most active member of the family of zebrafish RNases, its high activity could be due to the concomitant occurrence of an unobstructed B1 subsite, a feature found also in ZF-RNase-3, and of a cluster of positive charges at the N-terminal helix. In the neighbourhood of the catalytic histidine (His10) this cluster could help in substrate recognition.

The structural differences noted among the different members of the zebrafish RNase subfamily, in particular at the C-terminal region, roughly correlate with their thermodynamic behavior. The presence of the pseudo type II' beta-bend in ZF-RNase-2 and ZF-RNase-5 but not in ZF-RNase-3 and ZF-RNase-1 may be the source of their slightly different thermal stability. This feature is not present in the modeled structure of ZF-RNase-4, which also has a shorter N terminal helix. Its stability, comparable to that of ZF-RNase-2 and ZF-RNase-5, may well be due to the compactness of the protein and in particular to the shorter length of the loop connecting helix II to the beta strand next in the sequence, a feature that the enzyme shares with hANG and RNase A.

As for the bactericidal activity of zebrafish RNases, we have completed the inspection of all known ZF-RNases and found that they are all bactericidal, especially on Gram-negative bacteria. However, the most relevant result is the finding that their bactericidal activity is preserved not only after inactivation of their ribonucleolytic activity, but also after denaturation of the proteins. Clearly, the finding that bactericidal RNases do not use their ribonucleolytic activity for killing bacteria is not new, as it has been reported also for other bactericidal RNases [31-33]. Certainly surprising is instead the finding that they can perform a biological function, such as host-defence, a mechanism of innate immunity, while devoid of any structure. This question has been previously discussed for salmon RNases [6], which present the same behaviour. Apparently, the proteins can bind and penetrate the bacterial membrane also when unfolded, possibly for the presence in their amino acid sequences of many positively charged residues, which could form clusters that can readily act on the negatively charged outer leaflet of the bacterial membrane [31].

The finding of RNases in the phylogenetically distant fish proteome, and their ability to exert both angiogenic and bactericidal activity, has led to different proposals: that the earliest function of RNases in evolution was to promote angiogenesis [1], or to act as host defence effectors [3]. In fact, it cannot be excluded – in a gene sharing fashion [34]– that ancestral RNases were involved both in angiogenesis and host defence. Certainly surprising is the conclusion that these ancestral host- defence effectors evolved into the ordered RNase structure although they did not require this structure to exert their activity; on the other hand, the angiogenic activity could be exerted only by exploiting an RNase active site inside a well ordered RNase structure.

In conclusion, the data presented here on the structure of ZF-RNases, their thermodynamic stability, and on the relationships between their structure and their RNase activity, as well as the data on their bactericidal and angiogenic activity, and on their expression early in development,

provide an enlarged, more comprehensive picture of the zebrafish RNases, by adding many *tesserae* towards a complete mosaic.

EXPERIMENTAL

Cloning, expression and purification of recombinant ZF-RNases

ZF-RNases -1, -2 and -3 were produced as described in Pizzo *et al*. [5]. A plasmidic vector containing the gene sequence encoding ZF-RNase-4 was kindly provided by Dr. Zhang, University of Michigan, USA). To amplify the mature portion of the gene sequence, the following primers were used:

5'- TC**CATATG**CAGTCTTATAATGACTTCAAACGC-3' (forward)

5'-CCC**AAGCTT**TTAAGAATTGTTGGAACGTCCATA-3' (reverse)

Underlined letters indicate restriction sites added to perform cloning. The gene sequence encoding Zf-RNase-5 was obtained by PCR using as a template a cDNA clone (IMAGp998L1415615Q) purchased from ImaGenes (Berlin, Germany). To amplify the gene sequence, the following primers were used:

5'-GAAATTC**CATATG**AAGGTTCCACCAGACGTA-3' (forward)

5'-CCC**AAGCTT**TATTTAGCCTGACCTGTTTAC-3' (reverse)

Underlined letters indicate restriction sites added to perform cloning. The signal peptides of ZF-RNase-4 and ZF-RNase-5 were predicted using the signalp 3.0 server (http://www.cbs.dtu.dk/services/SignalP/).

The PCR reactions were performed under the following conditions: an initial denaturation step at 94 ^{o}C for 5 min, followed by 35 cycles of 2 min at 94 °C, 2 min at 62 °C, and 1 min at 73 °C. PCR products were isolated by electrophoresis on low melting 1% agarose gel, and purified using the Product Purification Kit (Roche Applied Science, Monza, Italy). Purified DNA, treated with NdeI and HindIII restriction enzymes, was inserted into the pET22b$^{(+)}$ expression vector. All cloned, purified DNAs were certified through sequencing (MWG Biotech, Edersberg, Germany) before processing.

The recombinant expression plasmids, with the exception of pET22b$^{(+)}$/ZF-RNase-4, were used to transform competent *E. coli* strain BL21(DE3) (provided by Invitrogen). The expression plasmid encoding ZF-RNase-4 was used to transform competent *E. coli* strain C43(DE3). (Invitrogen). Cells were grown at 37 °C to an A_{600} = 1 and then induced with 0.1 M isopropyl-1-thio-d-galactopyranoside and grown overnight.

The purification of the five recombinant ZF-RNases was carried out as previously described in Pizzo et al [5]. Briefly, inclusion bodies were solubilized in 7 M guanidine-HCl, 100 mM Tris acetate, pH 8.4 containing 1 mM glutathione. After flushing nitrogen for 10 min, each preparation was left for 2 h at room temperature. Renaturation was obtained through an initial dilution 1:20, drop by drop, in 100 mM Tris acetate, pH 8.4, containing 0.5 M L-arginine and 1 mM oxidized glutathione. After 24 h at room temperature, each preparation was dialyzed against 50 mM Tris-HCl, pH 7.4, and loaded on an SP-Sepharose column (GE Healthcare) equilibrated in the same buffer. Elution was carried out with a gradient from 0 to 1 M NaCl in the same buffer. The fractions containing ZF-RNases were revealed through SDS-PAGE followed by zymograms and pooled. To remove residual contaminants, each fraction pool was loaded on a reverse-phase C-4 column (Phenomenex) equilibrated in 100% solution A (5% acetonitrile, v/v, and 0.1% v/v, trifluoroacetic acid). The column was eluted with a gradient in which the concentration of solution B (composed of 90% acetonitrile containing 0.1% trifluoroacetic acid) was raised to 100% in 1 h. For each preparation a single, major protein component was eluted, which by SDS-PAGE was found to contain a single protein.

Assays of bactericidal activity

Bacterial strains of *E. coli* strain DH5α, *Pseudomonas fluorescens* (ATCC 13525), *Staphylococcus aureus* (ATCC 6538P) and *Bacillus subtilis* (PY79) were used in the antibacterial tests, performed as previously described [33]. The bacteria were grown overnight, diluted 1:1000 in 20 mM Na phosphate buffer (pH 7.0) and incubated with 3μM (final concentration) of ZF-RNase at a density of 4,000 colony-forming units (CFUs) per mL. After 6 h at 37° C, serial dilutions of each protein-bacteria mix were prepared and plated, and CFUs remaining after each treatment were determined. Negative controls were carried out with proteins from *E. coli* strain BL21(DE3) transformed with an empty pET22b$^{(+)}$ vector. For each experiment, carried out in duplicate, triplicate assays were performed. Standard deviations were 4-10 %, or as detailed for each experiment. LD_{50} values (the concentrations required for a 50% bactericidal effect) were determined by bactericidal assays at increasing concentrations up to 2 μM for each of the five RNases.

RT-PCR Experiments

Temporal expression patterns of ZF-RNases were determined by RT-PCR on total RNAs extracted from embryos at different development stages with the RNeasy Protect Mini Kit (Quiagen, Hilden, Germany). Total RNA (1 μg) from each time point was reverse transcribed to cDNA with the QIAGEN OneStep RT-PCR Kit following the manufacturer's instructions. cDNAs were amplified using the following specific primers:

For ZF-RNase-1:
5'-TTTATTCATAACGCTGCTTTTCA (forward);
5'- CCATGTTGCCCTGTGGAC-3' (reverse).
For ZF-RNase-2:
5'-TCACAACAGTGCTGTTCAATACA-3'(forward);
5'- TTCGTGTCGACCACCCGAT-3'(reverse).
For ZF-RNase-3:
5'-ACTTACGGTCAACCAGCAGAA-3' (forward);
5'- ACAAGTCTCTGTTATCAGTTTGTCG -3'(reverse);
For ZF-RNase-4:
5'-CCTGGGTTTAATTACCAGATTTC -3' (forward);
5'- CAATTATGTTTTCTATTTTGGTGCAG-3' (reverse).
For ZF-RNase-5:
5'-AAAAGACAACACTTCAGTCAAAAGG-3';
5'- AAACAGGTTGTTCACCGGAG-3' (reverse).
For *ZF-odc1*:
5'-TTGCAATCAAATCTTGAACAAA-3' (forward);
5'- GGAGGTGCTTCTTCAGGACA-3' (reverse).

All pairs of gene-specific primers were engineered to anneal to two different exons so that cDNA amplifications could be distinguished by product size, and from genomic contaminant amplifications. PCR reactions were carried out using 1 μL cDNA as template, 10 pmol of each primer, 1.25 U Taq DNA polymerase (Fermentas, Burlington, Ontario, Canada) in a total volume of 25 μL, under the following conditions: one cycle at 94 °C for 5 min followed by 35 cycles (40 for ZF-RNase-2 and -4) of 20 sec at 94 °C, 30 sec at 60 °C and 40 sec at 72 °C, with a final cycle at 72 °C for 7 min.

Angiogenesis assays

HUVE cells, cultured in EBM-2 basal endothelial cell culture medium containing the EGM-2 Bullet kit (Cambrex Corp., East Rutherford, NJ, USA), were seeded in Matrigel-coated 48-well plates (Becton-Dickinson Biosciences, Franklin Lakes, NJ, USA) at a density of $4x10^4$ cells per well in 150 μL of EBM-2 basal medium. ZF-RNase-4, ZF-RNAse-5 and recombinant human angiogenin were added to the cells at different concentrations and incubated at 37 °C for 4 h. Cells were fixed with phosphate-buffered glutaraldehyde (0.2%) and paraformaldehyde (1%), and photographed.

Assays of RNase activity

Zymogram assays of RNase activity were carried out on SDS /PAGE electropherograms as described previously (Blank et al 1982). Ribonucleolytic assays in vitro were carried as described by Kelemen, B. R. et al. [24] with a fluorogenic substrate: 6-carboxy-fluorescein-dArUdAdA-6-carboxy-tetramethylrhodamine (Integrated DNA Technologies, Coralville, IA, USA). The assay mixtures contained 0.1 M imidazole-HCl (pH 6.0), 0.1 M NaCl, 20–60 nM substrate, and suitable enzyme aliquots. All preparations were checked for constant specific activity with the in vitro assay indicated above before using them for any biological or physico-chemical test.

Chemical and physical denaturation of ZF-RNases

Reduced and alkylated ZF-RNases were obtained by treating ZF-RNases (1 mg/ml) for 2 h at 37°C with a 10-fold molar excess of dithiothreitol in 200 mM MES-NaOH pH 6.0. Carboxymethylation of the exposed sulfhydryls was carried out by adding a 20-fold molar excess (with respect to total –SH concentration) of iodoacetamide. After 60 min at room temperature in the dark the protein was freed of excess reagents and by-products by gel filtration through a PD10 column (GE Healthcare Bioscience AB, Uppsala, Sweden) equilibrated in 0.1 M ammonium acetate at pH 5, and lyophilized. Mass spectrometry analyses revealed an increase of molecular weight consistent with the effects of the carboxymethylation reaction.

Thermal denaturation of ZF-RNases was achieved by treating the proteins for 5 min at 85 °C, followed by rapid cooling to 0 °C.

CD Spectroscopy

CD measurements were carried out on a Jasco J-715 spectropolarimeter equipped with a Peltier-type temperature control system (model PTC-348WI). Molar ellipticity per mean residue, [θ] in degrees cm^2 $dmol^{-1}$, was calculated from the equation $[\theta] = [\theta]_{obs}mrw/10lC$, where $[\theta]_{obs}$ is the ellipticity measured in degrees, mrw is the mean residue molecular mass (117 Da), l is the optical path length of the cell in cm and C is the protein concentration in $mol \cdot L^{-1}$. A 0.1-cm path length cell and a protein concentration of 0.2 mg mL^{-1} in 10 mm Na phosphate buffer (pH 7.2), were used. CD spectra were recorded at 25 °C in a 0.1-cm quartz cell, averaged over three scans from 260 to 190 nm with a time constant of 16 s, a 2-nm band width, and a scan rate of 20 nm min^{-1}. CD spectra were baseline-corrected by subtracting the buffer spectrum. The instrument was calibrated with an aqueous solution of D-10-camphorsulfonic acid at 290 nm [35]. Thermal unfolding was monitored in the temperature scan mode at 222 nm from 25 °C up to 85 °C with a scan rate of 1^oC min^{-1}.

The fraction of denatured protein (Δf_D) was calculated as: $\Delta f_D = (\Theta-\Theta min)/(\Theta max-\Theta min)$; Θ is the ellipticity at a given temperature, Θ_{max} and Θ_{min} the maximum and minimum values of ellipticity corresponding to the denatured and native states of the proteins, respectively.

The urea-induced transition curves were obtained by recording the ellipticity at 222 nm as a function of denaturant concentration. Measurements were performed after overnight incubation of samples at 4 °C. The protein concentration was 0.2 mg mL^{-1}. The enthalpy changes were calculated fitting CD melting curves by the van't Hoff equation using the Origin 7.5 program.

Fluorescence spectroscopy

Intrinsic protein fluorescence was recorded using a Jasco FP-750 spectrofluorimeter equipped with a circulating water bath. The excitation wavelength was set at 280 nm, and the emission was measured between 300 and 450 nm. The spectra were recorded at room temperature with a 1 cm cell and a 5 nm emission slit width, and were corrected for background signal.

The urea-induced transition curves were obtained by recording fluorescence intensity at the wavelength maximum as a function of denaturant concentration. As for CD measurements, fluorescence measurements were performed after overnight incubation of samples at 4 °C at a protein concentration 0.2 mg mL^{-1}.

Differential Scanning Calorimetry

DSC measurements were carried out on a third generation Setaram Micro-DSC. A scanning rate of 0.5 °C min^{-1} was chosen for all experiments. 2 mg mL^{-1} protein solutions were prepared in 10 mM sodium phosphate buffer at pH 7.2. Raw data were converted into an apparent molar heat capacity taking into account the instrument calibration curve and the buffer–buffer scanning curve, and by dividing each data point by the scan rate and the protein molar concentration in the sample cell. Reheating runs were repeated to determine the calorimetric reversibility of the thermal-denaturation process. The excess molar heat capacity function, $< \Delta C_p^0 >$, was obtained after baseline subtraction, assuming as reference the heat capacity of the native state [36]. The denaturation enthalpies, ΔH_{cal}^0, were obtained by integrating the area under the heat capacity versus temperature curves. T_m is the melting temperature and corresponds to the maximum of each DSC peak. The entropy changes, ΔS_{cal}^0, were determined by integrating the curve obtained by dividing the heat capacity curve by the absolute temperature. The denaturation enthalpies, entropies and Gibbs energies at 298 K were calculated according to the classical Kirchhoff equations.

Crystallization and diffraction procedures

Crystals of ZF-RNase-1 were obtained by hanging drop vapour diffusion method. Drops were prepared at 20 °C by mixing equal volumes of protein solution (15 mg/ml) and reservoir solution containing 1.8-2 M ammonium sulphate and 0.1 M sodium acetate pH 4.2-4.8 (ZF1_pH4.5). To analyze the structure of ZF-RNase-1 at higher pH, the crystals, grown at pH 4.5, were transferred to harvesting solutions (2.3 M ammonium sulphate) buffered, at pH values in the range 4.5 - 7.3. A stepwise procedure in which the pH was adjusted in steps of 0.2 was necessary to avoid deterioration of crystal quality. Crystals were stored under the final pH condition (ZF1_pH7.3) for a week with daily changes of the mother liquor.

The best crystals of ZF-RNase-5 were obtained using the hanging drop vapour diffusion method by mixing equal volumes of protein (15 mg/ml) and precipitant solution containing 32 % w/v MPEG 2000, 0.1 M sodium acetate (pH 4.5) and 0.2 M ammonium sulphate.

Diffraction data of ZF1_pH4.5 were collected by using synchrotron light at ELETTRA, Trieste. In the other two cases, data were collected on a Saturn944 CCD detector with a Cu $K\alpha$ radiation from a Rigaku Micromax 007 HF generator. In all cases, after the addition of 30 % w/v glycerol to the harvesting solution, crystals were flash-frozen at 100 K in supercooled N2 gas produced by an Oxford Cryosystem and maintained at 100 K during the data collection. All data were indexed, processed and scaled using the HKL2000 package [37].

Structure determination

The structure of ZF1_pH4.5 was solved by molecular replacement, using the program "Phaser" [38] and the model of the homologous bovine angiogenin (PDB code 1AGI) [29], as the structure of the protein determined at pH 8.0 (ZF1_pH8) [4], was not yet available. Phaser program was also employed to solve the structure of ZF-RNase-5 using ZF1_pH4.5 as starting model.

Refinement was carried out with CNS [39]. Each refinement step was followed by manual interventions using the program O [40] to correct minor errors in the positions of some side chains and to identify solvent sites. The final models of ZF1_pH4.5, ZF1_pH7.3 and ZF-RNase-5, have an R-factor (R-free) of 0.162 (0.192), 0.152 (0.205) and 0.178 (0.210), respectively. They have been deposited in the Protein Data Bank (Codes 3LJD, 3LN8 and 3LJE, respectively.). Statistics and parameters of the refinements are given in Table 2.

All the structures were validated with PROCHECK [41] and WHATCHECK [42].Cartoons were generated using Pymol (http://pymol.org).

Homology modelling

The structures of ZF-RNase-2 and ZF-RNase-4 were modelled with the SWISS-MODEL server [43], using as reference the crystal structure of Zf-RNase-5 and ZF-RNase-3, respectively. The templates were chosen on the basis of the highest score and the lowest E-value found with a BLAST search against the PDB database. Positional sequence identity between ZF-RNase-2 and

ZF-RNase-5 was 73%, whereas that between ZF-RNase-4 and ZF-RNase-3 was 33%. The models produced by the server were then manually adjusted to built missing residues on the N-terminal α-helical region and energy-minimized in vacuo by means of the GROMOS96 force-field, following a procedure previously reported [44,45].

The stereochemical quality of the final models showed no residues positioned in the disallowed regions of the Ramachandran plot. The *Z*-score values of the combined statistical potential energy of the ZF-RNase-2 and ZF-RNase-4 models were -6.04 and -5.12, respectively. These values are in the range of scores typically found in proteins of similar sequence length and are analogous to the values of the templates which are equal to –6.22 and –6.30, respectively.

The *Z*-score indicates overall model quality and measures the deviation of the total energy of the structure with respect to an energy distribution derived from random conformations [46,47].

ACKNOWLEDGMENTS

This study was supported by the Ministero Italiano dell'Università e della Ricerca Scientifica (PRIN 2007).The authors thank Giosuè Sorrentino and Maurizio Amendola for technical assistance; Elettra Trieste for providing synchrotron radiation facilities, Dr. Antimo Di Maro for mass spectrometry analyses, and Gaetano D'Amato for preparing zebrafish RNAs.

REFERENCES

[1] Pizzo, E. and D'Alessio, G. (2007). The success of the RNase scaffold in the advance of biosciences and in evolution. Gene 406, 8-12.

[2] Lander, E.S. et al. (2001). Initial sequencing and analysis of the human genome. Nature 409, 860-921.

[3] Cho, S. and Zhang, J. (2007). Zebrafish ribonucleases are bactericidal: implications for the origin of the vertebrate RNase A superfamily. Mol. Biol. Evol. 24, 1259-68.

[4] Kazakou, K., Holloway, D.E., Prior, S.H., Subramanian, V. and Acharya, K.R. (2008). Ribonuclease A homologues of the zebrafish: polymorphism, crystal structures of two representatives and their evolutionary implications. J. Mol. Biol. 380, 206-22.

[5] Pizzo, E., Buonanno, P., Di Maro, A., Ponticelli, S., De Falco, S., Quarto, N., Cubellis, M.V. and D'Alessio, G. (2006). Ribonucleases and angiogenins from fish. J. Biol. Chem. 281, 27454-60.

[6] Pizzo, E., Varcamonti, M., Di Maro, A., Zanfardino, A., Giancola, C. and D'Alessio, G. (2008). Ribonucleases with angiogenic and bactericidal activities from the Atlantic salmon. FEBS J. 275, 1283-95.

[7] Kishikawa, H., Wu, D. and Hu, G.F. (2008). Targeting angiogenin in therapy of amyotropic lateral sclerosis. Expert Opin. Ther. Targets 12, 1229-42.

[8] Fu, H. et al. (2009). Stress induces tRNA cleavage by angiogenin in mammalian cells. FEBS Lett. 583, 437-42.

[9] Yamasaki, S., Ivanov, P., Hu, G.F. and Anderson, P. (2009). Angiogenin cleaves tRNA and promotes stress-induced translational repression. J. Cell. Biol. 185, 35-42.

[10] Quarto, N., Pizzo, E. and D'Alessio, G. (2008). Temporal and spatial expression of RNases from zebrafish (Danio rerio). Gene 427, 32-41.

[11] Covassin, L.D., Siekmann, A.F., Kacergis, M.C., Laver, E., Moore, J.C., Villefranc, J.A., Weinstein, B.M. and Lawson, N.D. (2009). A genetic screen for vascular mutants in zebrafish reveals dynamic roles for Vegf/Plcg1 signaling during artery development. Dev. Biol. 329, 212-26.

[12] Lawson, N.D. and Weinstein, B.M. (2002). Arteries and veins: making a difference with zebrafish. Nat. Rev. Genet. 3, 674-82.

[13] Ny, A., Autiero, M. and Carmeliet, P. (2006). Zebrafish and Xenopus tadpoles: small animal models to study angiogenesis and lymphangiogenesis. Exp. Cell. Res. 312, 684-93.

[14] Monti, D.M. et al. (2009). Characterization of the angiogenic activity of zebrafish ribonucleases. FEBS J. 276, 4077-90.

[15] Berisio, R., Lamzin, V.S., Sica, F., Wilson, K.S., Zagari, A. and Mazzarella, L. (1999). Protein titration in the crystal state. J. Mol. Biol. 292, 845-54.

[16] Holloway, D.E., Chavali, G.B., Hares, M.C., Subramanian, V. and Acharya, K.R. (2005). Structure of murine angiogenin: features of the substrate- and cell-binding regions and prospects for inhibitor-binding studies. Acta Crystallogr D Biol. Crystallogr. 61, 1568-78.

[17] Leonidas, D.D., Chavali, G.B., Jardine, A.M., Li, S., Shapiro, R. and Acharya, K.R. (2001). Binding of phosphate and pyrophosphate ions at the active site of human angiogenin as revealed by X-ray crystallography. Protein Sci. 10, 1669-76.

[18] Vitagliano, L., Merlino, A., Zagari, A. and Mazzarella, L. (2000). Productive and nonproductive binding to ribonuclease A: X-ray structure of two complexes with uridylyl(2',5')guanosine. Protein Sci. 9, 1217-25.

[19] Mazzarella, L., Capasso, S., Demasi, D., Di Lorenzo, G., Mattia, C.A. and Zagari, A. (1993). Bovine Seminal Ribonuclease. Structure at 1.9 Å resolution. Acta Crystallogr. D49, 389-402.
[20] Merlino, A., Mazzarella, L., Carannante, A., Di Fiore, A., Di Donato, A., Notomista, E. and Sica, F. (2005). The importance of dynamic effects on the enzyme activity: X-ray structure and molecular dynamics of onconase mutants. J. Biol. Chem. 280, 17953-60.
[21] Merlino, A., Vitagliano, L., Sica, F., Zagari, A. and Mazzarella, L. (2004). Population shift vs induced fit: the case of bovine seminal ribonuclease swapping dimer. Biopolymers 73, 689-95.
[22] Barone, G., Catanzano, F., Del Vecchio, P., Giancola, C. and Graziano, G. (1997). Thermodynamics of protein stability: a family of ribonucleases. . Pure & Applied Chemistry 69, 2307-2313.
[23] Crabtree, B. et al. (2007). Characterization of human angiogenin variants implicated in amyotrophic lateral sclerosis. Biochemistry 46, 11810-8.
[24] Kelemen, B.R., Klink, T.A., Behlke, M.A., Eubanks, S.R., Leland, P.A. and Raines, R.T. (1999). Hypersensitive substrate for ribonucleases. Nucleic Acids Res. 27, 3696-701.
[25] Leland, P.A., Staniszewski, K.E., Park, C., Kelemen, B.R. and Raines, R.T. (2002). The ribonucleolytic activity of angiogenin. Biochemistry 41, 1343-50.
[26] Zanfardino, A., Pizzo, E., Di Maro, A., Varcamonti, M. and D'Alessio, G. (2010). The bactericidal action on Escherichia coli of ZF-RNase-3 is triggered by the suicidal action of the bacterium OmpT protease. Febs J. 277, 1921-8.
[27] Moussaoui, M., Guasch, A., Boix, E., Cuchillo, C. and Nogues, M. (1996). The role of non-catalytic binding subsites in the endonuclease activity of bovine pancreatic ribonuclease A. J. Biol. Chem. 271, 4687-92.
[28] Acharya, K.R., Shapiro, R., Allen, S.C., Riordan, J.F. and Vallee, B.L. (1994). Crystal structure of human angiogenin reveals the structural basis for its functional divergence from ribonuclease. Proc. Natl. Acad. Sci U S A 91, 2915-9.
[29] Acharya, K.R., Shapiro, R., Riordan, J.F. and Vallee, B.L. (1995). Crystal structure of bovine angiogenin at 1.5-A resolution. Proc. Natl. Acad. Sci U S A 92, 2949-53.
[30] Schultz, L.W., Quirk, D.J. and Raines, R.T. (1998). His...Asp catalytic dyad of ribonuclease A: structure and function of the wild-type, D121N, and D121A enzymes. Biochemistry 37, 8886-98.
[31] Huang, Y.C. et al. (2007). The flexible and clustered lysine residues of human ribonuclease 7 are critical for membrane permeability and antimicrobial activity. J. Biol. Chem. 282, 4626-33.
[32] Nitto, T., Dyer, K.D., Czapiga, M. and Rosenberg, H.F. (2006). Evolution and function of leukocyte RNase A ribonucleases of the avian species, Gallus gallus. J. Biol. Chem. 281, 25622-34.
[33] Rosenberg, H.F. (1995). Recombinant human eosinophil cationic protein. Ribonuclease activity is not essential for cytotoxicity. J. Biol. Chem. 270, 7876-81.
[34] Piatigorsky, J. and Wistow, G. (1991). The recruitment of crystallins: new functions precede gene duplication. Science 252, 1078-1079.
[35] Venyaminov, S.Y. and Yang, J.T. (1996) Determination of protein secondary structure. In Circular Dichroism and the Conformational Analysis of Biomolecules (Fasman, G.D., ed.^eds), pp. 69–107. Plenum Press New York.
[36] Barone, G., Del Vecchio, P., Fessas, D., Giancola, C. and Graziano, G. (1993). THESEUS: A New Software Package for the Handling and Analysis of Thermal Denaturation Data for Biological Macromolecules. J.Thermal Anal. 39, 2779-2790.
[37] Otwinowsky, Z. and Minor, W. (1997) Processing of X-ray diffraction data collected in oscillation mode In Methods in Enzymology (C.W. Carter, J. and Sweet, R.M., ed.^eds), pp. 307-326

[38] McCoy, A.J., Grosse-Kunstleve, R.W., Storoni, L.C. and Read, R.J. (2005). Likelihood-enhanced fast translation functions. Acta Crystallogr D Biol Crystallogr 61, 458-64.
[39] Brunger, A.T. et al. (1998). Crystallography & NMR system: A new software suite for macromolecular structure determination. Acta Crystallogr D Biol Crystallogr 54, 905-21.
[40] Jones, T.A., Zou, J.Y., Cowan, S.W. and Kjedgaard, M. (1991). Improved methods for binding protein models in electron density maps and the location of errors in these models. Acta Cryst. D: Biol. Cryst. 56, 714-721.
[41] Laskowski, R.A., MacArthur, M.W., Moss, M.D. and Thornton, J.M. (1993). PROCHECK: A program to check the stereochemical quality of protein structure. ;. J. Appl. Crystallogr. 26, 283-291.
[42] Hooft, R.W., Vriend, G., Sander, C. and Abola, E.E. (1996). Errors in protein structures. Nature 381, 272.
[43] Schwede, T., Kopp, J., Guex, N. and Peitsch, M.C. (2003). SWISS-MODEL: An automated protein homology-modeling server. Nucleic Acids Res. 31, 3381-5.
[44] Merlino, A., Graziano, G. and Mazzarella, L. (2004). Structural and dynamic effects of alpha-helix deletion in Sso7d: implications for protein thermal stability. Proteins 57, 692-701.
[45] Porcelli, M., Moretti, M.A., Concilio, L., Forte, S., Merlino, A., Graziano, G. and Cacciapuoti, G. (2005). S-adenosylhomocysteine hydrolase from the archaeon Pyrococcus furiosus: biochemical characterization and analysis of protein structure by comparative molecular modeling. Proteins 58, 815-25.
[46] Sippl, M.J. (1993). Recognition of errors in three-dimensional structures of proteins. Proteins 17, 355-62.
[47] Sippl, M.J. (1995). Knowledge-based potentials for proteins. Curr. Opin. Struct. Biol. 5, 229-35.
[48] Kabsch, W. and Sander, C. (1983). Dictionary of protein secondary structure: pattern recognition of hydrogen-bonded and geometrical features. Biopolymers 22, 2577-637.

TABLE 1
Nomenclatures of zebrafish RNases

Zebrafish RNases		
ZF-RNase-1[a]		RNase ZF-1a[c]
ZF-RNase-2[a]	*Dr*-RNase 2[b]	RNase ZF-2a[c]
ZF-RNase-3[a]	*Dr*-RNase 1[b]	RNase ZF-3e[c]
ZF-RNase-4[a]	*Dr*-RNase 3[b]	RNase ZF-4[c]
ZF-RNase-5[a]		RNase ZF-2b[c]

[a] The nomenclature used by Pizzo et al. [5]
[b] The nomenclature used by Cho and Zhang [3]
[c] The nomenclature used by Kazaukou et al. [4]

TABLE 2 Data collection and refinement statistics

	ZF1_pH4.5	ZF1_pH7.3	ZF-RNase-5
Space group	P212121	P212121	I4132
Cell parameters			
a (Å)	41.34	41.57	126.49
b (Å)	48.97	49.18	126.49
c (Å)	109.91	110.28	126.49
Resolution limits (Å)	30.00-1.38	30.00-1.61	50.00-1.80
Highest resolution shell (Å)	1.42-1.38	1.67-1.61	1.86-1.80
No. of observations	430152	451397	913538
No. of unique reflections	41877	28093	16327
Completeness (%)	89.7 (54.1)	93.3 (51.4)	99.9 (99.9)
I/σ (I)	29 (2)	24 (5)	24 (3)
Average multiplicity	3.2	4.9	10.0
Rmerge (%)	4.9 (38.5)	5.4 (11.5)	9.5 (64.8)
Mosaicity	0.43	0.65	0.52
Refinement Results			
Resolution limits (Å)	30.00-1.38	30.00-1.61	50.00-1.80
Number of reflections used in the refinement (F>2σ(F))	40180	27488	15282
No. of reflections in working set	36128	24765	13762
No. of reflections in test set	4052	2723	1520
Rworking/Rfree (%)	16.2/19.2	15.2/20.5	17.8/21.0
No. of protein atoms	2075	2084	969
Ligand atoms and water molecules	458	434	127
RMSD from ideal values			
Bond lengths (Å)	0.027	0.028	0.031
Bond angles (°)	2.4	2.4	2.5
Average B-factors (Å^2)			
Protein, overall	15.63	13.55	24.96
Main chains	13.67	11.53	23.61
Side chains	17.50	15.43	26.30
Solvent atoms	36.06	30.42	38.29
Ion atoms	33.06	36.15	41.36

Note: Values in parentheses correspond to the highest resolution shells.

TABLE 3

Physicochemical parameters of ZF-RNases, human angiogenin (hANG) and RNase A. C½ values were the urea concentrations at half-completion of the transition.

	T_m * (°C)	T_m ** (°C)	ΔH^0_{cal} (kJmol^{-1})	$\Delta H^0_{v.H.}$ (kJmol^{-1})	ΔS^0_{cal} (kJK^{-1}mol^{-1})	ΔG^0_{298} (kJmol^{-1})	$C_{½}$* (M)	$C_{½}$*** (M)
ZF-RNasi-1	54.5	54.9	298	241	0.91	21	2.8	2.7
ZF-RNasi-2	63.6	63.8	360	325	1.07	27	5.2	5.0
ZF-RNasi -3	55.2	55.5	297	248	0.90	23	3.2	3.3
ZF-RNasi-4	64.0	64.8	366	330	1.08	29	4.5	4.6
ZF-RNasi-5	64.7	64.3	301	255	0.89	25	4.3	4.4
hANG	63.5	62.6	348	353	1.04	29	4.2	4.4
RNasi A	64.0	64.0	489	461	1.45	45	7.0	7.1

* Data from CD measurements; ** from DSC measurements; *** from fluorescence measurements. The error in T_m is ± 1 °C and ± 0.5 °C for CD and DSC measurements, respectively. The error in ΔH^0_{cal} and ΔS^0_{cal} is <5%. The error in $\Delta S^0_{v.H.l}$ is <10% and in ΔG^0_{298} <15%.

TABLE 4

Kinetic data on the ribonucleolytic activity of ZF-RNases, human angiogenin (hANG), and bovine pancreatic RNase A, the prototype of the vertebrate RNase superfamily.

	k_{cat}/K_M ($M^{-1} s^{-1}$)
ZF-RNase-1	$5.32 \pm 0.39 \cdot 10^2$
ZF-RNase-2	$1.91 \pm 0.13 \cdot 10^2$
ZF-RNase-3	$2.17 \pm 0.15 \cdot 10^3$
ZF-RNase-4	$0.91 \pm 0.05 \cdot 10^5$
ZF-RNase-5	$1.25 \pm 0.09 \cdot 10^4$
hANG	$1.72 \pm 0.12 \cdot 10^3$
RNase A	$8.40 \pm 0.46 \cdot 10^6$

LEGENDS FOR FIGURES

FIGURE 1.
Amino acid sequences of zebrafish RNases. Residues shared by all five zebrafish RNases and by human angiogenin are shown in black with a grey background, while the residues shared also by RNase A are shown in white character with a black background.

FIGURE 2**.**
Ribbon representation of the structures of ZF-RNases.

FIGURE 3. **A) Active site region of ZF-RNase-5.** The structure of ZF-RNase-5 (green) is superimposed to that of RNase A (pink) in complex with the ATAA tetranucleotide (violet).
B) Superimposition of the C-terminal region of ZF-RNase-5 (green) and RNase A (pink). The pseudo type II' beta-bend and the C_{10} hydrogen bond between Asp119 and Gly121 in ZF-RNase-5 are highlighted.

FIGURE 4**.**
Far-UV CD melting profiles recorded at 222 nm. A Δf_D value represents the fraction of denatured protein (see Experimental section). Symbols are as indicated in brackets: ZF-RNase-1 (triangle), ZF-RNase-2 (square), ZF-RNase-3(star), ZF-RNase-4 (bar), ZF-RNase-5 (circle), RNase A (dashed line), hANG (solid line).

FIGURE 5.
Angiogenic activity of ZF-RNase-4 and -5. Assays were carried out with primary human umbilical endothelial vein cells. *A*, negative412 control obtained with non-supplemented EBM-2 medium; *B*, human angiogenin (200 ng/ml); *C* and *D*, recombinant ZF-RNase-4 tested at 200 and 400 ng/ml; *E* and *F*, recombinant ZF-RNase-5 tested at 200 and 400 ng/ml.

FIGURE 6.
Bactericidal activity of ZF-RNases (3 μM final concentration) after incubation of bacterial cells for 6 h. Cell survival was determined as percent of controls, determined with bacteria untreated or treated with 3 μM bovine serum albumin. The average of 3 measurements is shown; standard error was lower than 5%. The bacteria were: A, *Escherichia coli*; B, *Pseudomonas fluorescens*; C, *Bacillus subtilis*; D, *Staphylococcus aureus.*

FIGURE 7.
Expression patterns of ZF-RNases during zebrafish embryo development. The assays were performed by RT-PCR. Total RNA, extracted from whole-body embryos at the indicated hours post-fertilization, was treated with DNase and retrotranscribed in cDNA. No expression was detectable for ZF-RNase-2 and -4. ZF-RNase-1, -3 and -5 are expressed at all analyzed stages. The expression of the housekeeping gene (ZF-odc1) was used as a positive control.

FIGURE 1

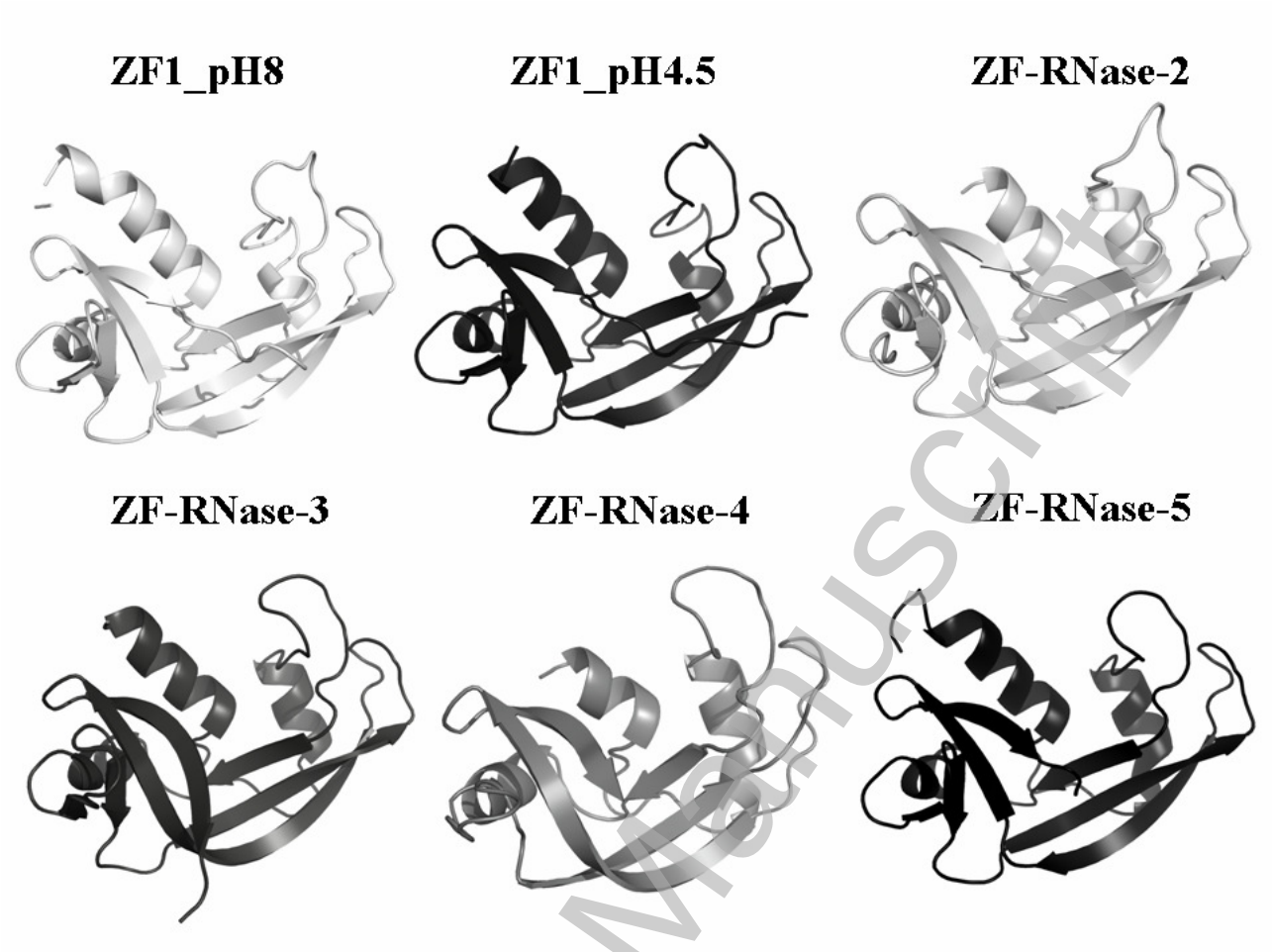

FIGURE 2

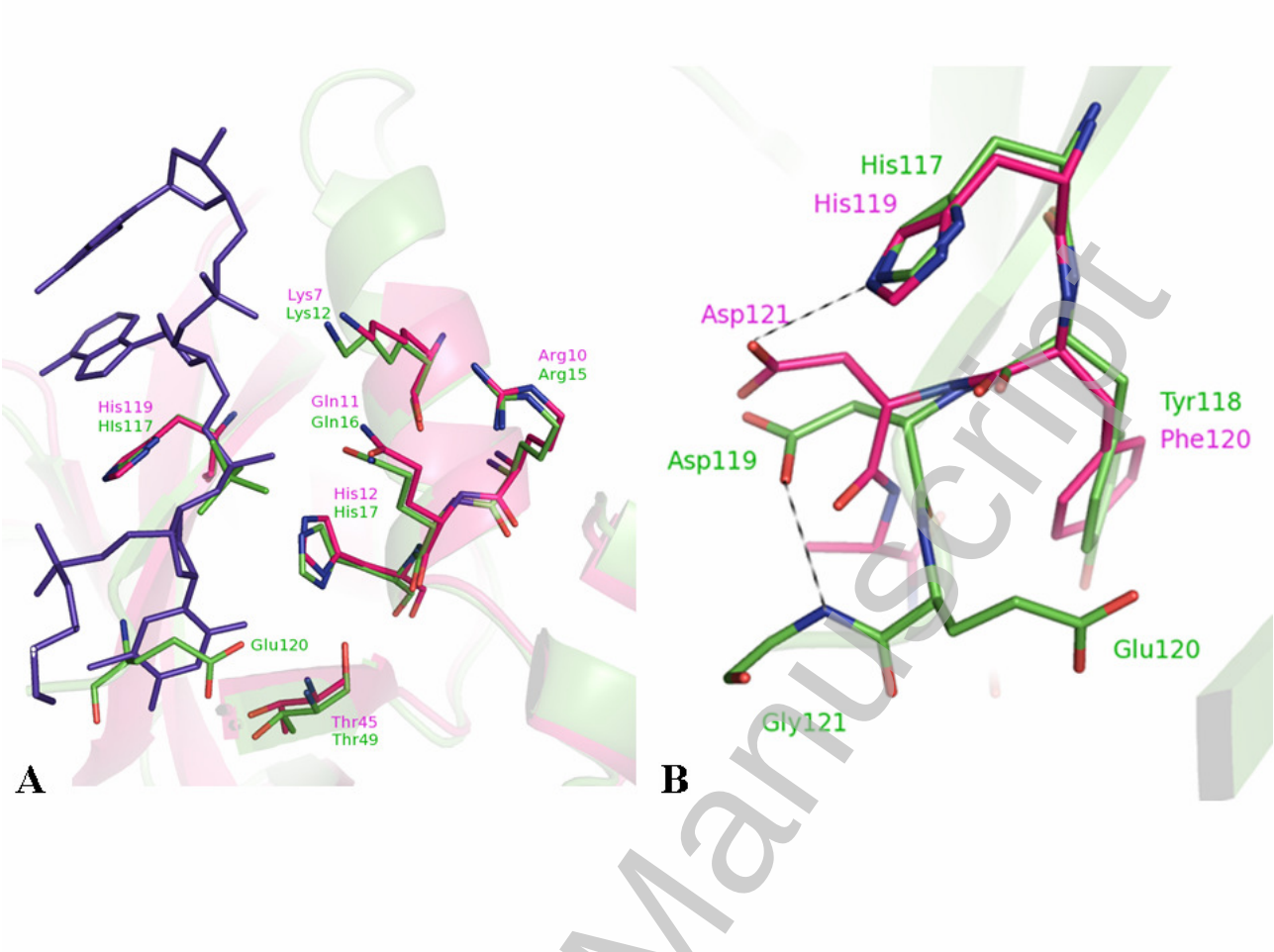

FIGURE 3

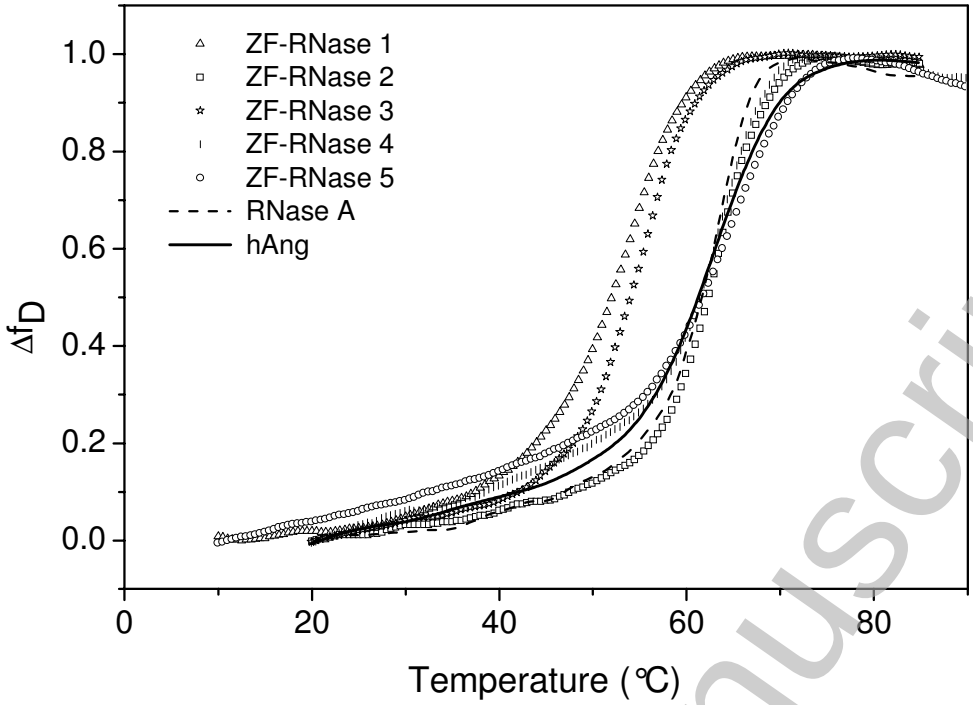

FIGURE 4

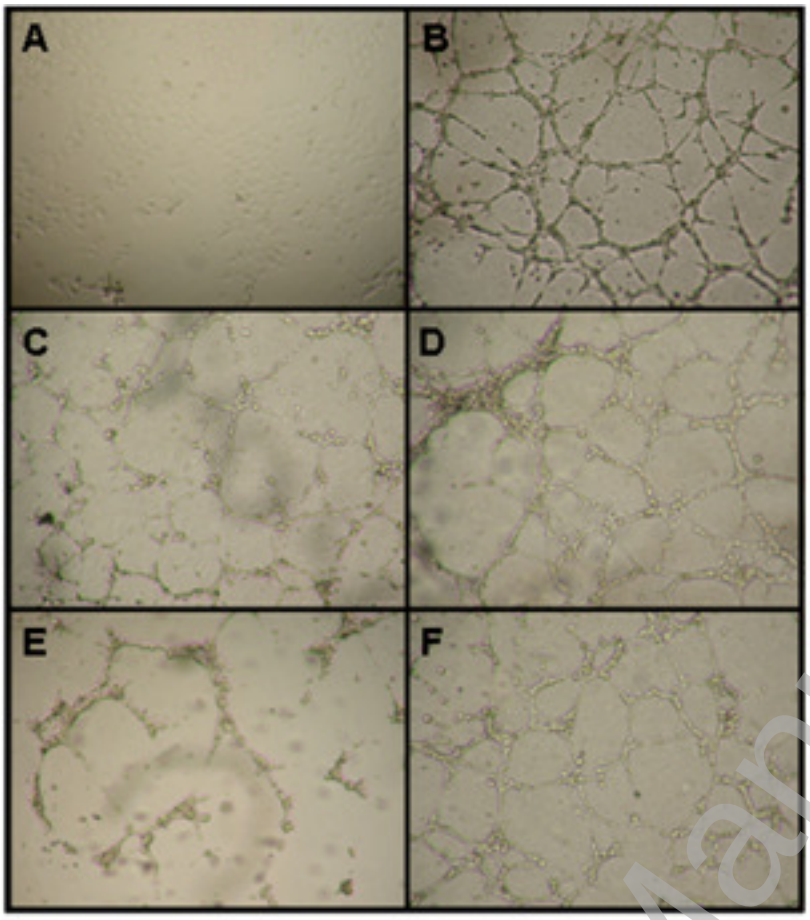

FIGURE 5

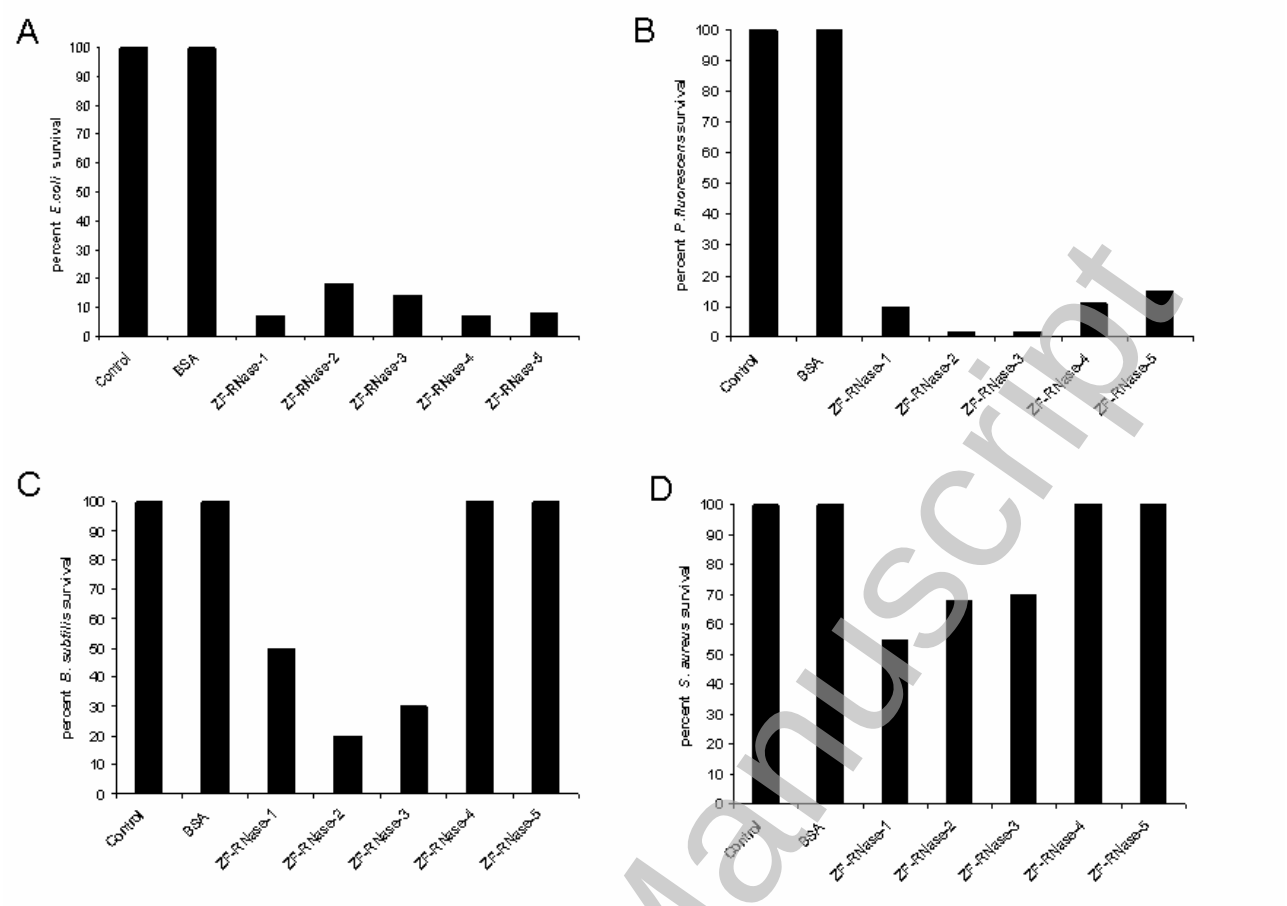

FIGURE 6

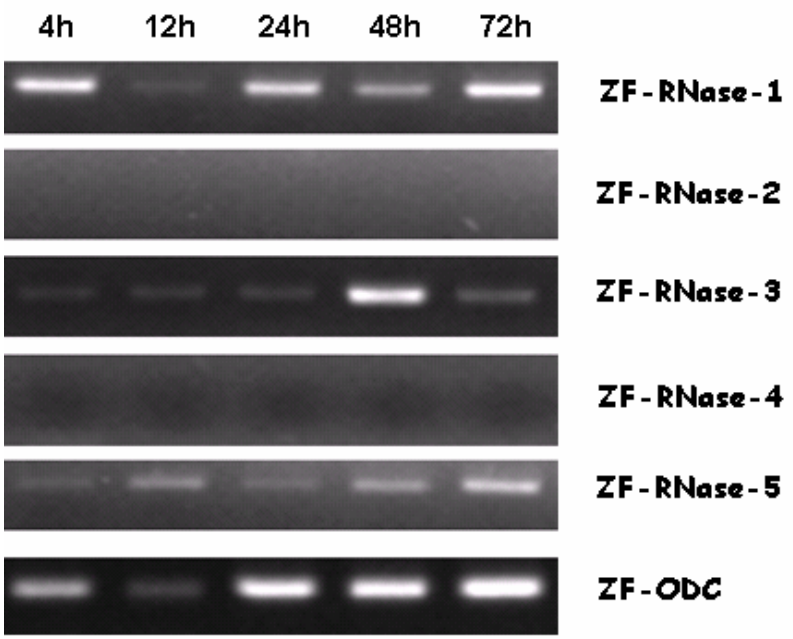

FIGURE 7